Hyperfine Interact
DOI 10.1007/s10751-011-0499-x

Manipulation of the heme electronic structure by external stimuli and ligand field

Yoshiki Ohgo · Masashi Takahashi · Kazuyuki Takahashi · Yukiko Namatame · Hisashi Konaka · Hatsumi Mori · Saburo Neya · Shinya Hayami · Daisuke Hashizume · Mikio Nakamura

© Springer Science+Business Media B.V. 2011

Abstract This review describes the switching behaviors of the electronic structure, which were observed in iron(III) porphyrinoids, by the addition of external stimuli. The combined analysis by various methods, such as EPR, Mössbauer, SQUID, single crystal X-ray structure analysis, revealed a wide variety of electronic structures of the heme related complexes. This paper focuses in particular on the spin-crossover

Y. Ohgo (✉) · M. Nakamura
Department of Chemistry, School of Medicine, Toho University, Ota-ku,
Tokyo 143-8540, Japan
e-mail: yohgo@med.toho-u.ac.jp

Y. Ohgo
Toho University Advanced Medical Research Center, Ota-ku, Tokyo 143-8540, Japan

Y. Ohgo · M. Takahashi · M. Nakamura
Division of Chemistry, Graduate School of Science, Toho University, Funabashi,
Chiba 274-8510, Japan

K. Takahashi · H. Mori
Institute for Solid State Physics, The University of Tokyo, Kashiwa,
Chiba 277-8581, Japan

Y. Namatame · H. Konaka
Rigaku Corporation, Akishima, Tokyo 196-8666, Japan

S. Neya
Department of Physical Chemistry, Graduate School of Pharmaceutical Sciences,
Chuoh-Inohana, Chiba, Chiba 260-8675, Japan

S. Hayami
Department of Chemistry, Graduate School of Science and Technology,
Kumamoto University, Kurokami, Kumamoto 860-8555, Japan

D. Hashizume
Advanced Technology Support Division, RIKEN-Advanced Science Institute, Wako,
Saitama 351-0198, Japan

Published online: 07 December 2011

phenomenon in the solid state. An overview of spin-crossover phenomena found in iron(III) porphyrinoids between (i) $S = 5/2$ and $S = 1/2$, (ii) $S = 3/2$ and $S = 1/2$, (iii) $S = 5/2$ and $S = 3/2$, will be described.

Keywords Spin-crossover · Iron(III) · Porphyrin · Porphyrinoid · Electronic structure

Abbreviations

Axial Ligands	
3-ClPy	3-chloropyridine;
1-MeIm	1-methylimidazole;
HIm	imidazole;
DMAP	4-(N,N-dimethylamino)pyridine;
4-CNPy	4-cyanopyridine;
Py	pyridine;
THF	tetrahydrofuran
Porphyrin dianioins	
OEP	dianions of 2,3,7,8,12,13,17,18-octaethylporphyrin;
TPP	dianions of 5,10,15,20-tetraphenylporphyrin;
OETPP	dianions of 2,3,7,8,12,13,17,18-octaethyl-5,10,15,20-tetraphenylporphyrin;
OETArP	dianions of 2,3,7,8,12,13,17,18-octaethyl-5,10,15,20-tetraarylporphyrins

1 Introduction

In biological systems, only sophisticatedly controlled systems have survived during the long evolutional process. Hence, investigations to clarify the orbital interactions or the nature of the chemical bonds between metals and ligands in the metalloproteins are quite important not only for understanding their functional activation mechanisms, but also for the development of related catalysts or functional materials in a biomimetic way. In this way hemeproteins have attracted much attention because of their wide variety of functions in spite of the same or similar prosthetic groups at the active center. One of the reasons for these versatile functions is the tailor made cavity around each heme provided by the unique protein matrix. The protein matrix manipulates the environment, such as the axial ligand field, around the heme, and the heme deformation, which switches the electronic structure of the heme to regulate its functions.

Another attractive characteristic is that the heme iron(III) ion can adopt various spin states such as $S = 5/2$, 3/2, and 1/2. Of the three spin states, $S = 5/2$ and $S = 1/2$ systems are very common both in models and bio-systems. On the other hand,

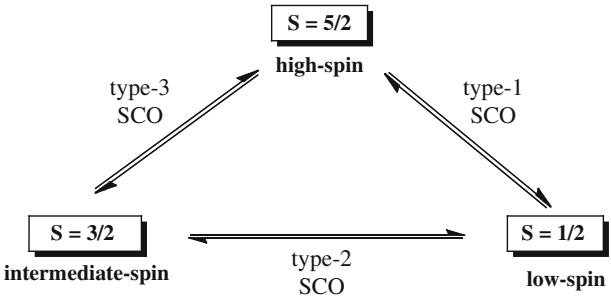

Scheme 1 Spin-crossover triangle in iron(III) porphyrinoids

$S = 3/2$ systems are less common because of the difficulty in tuning the ligand-field to obtain such complexes.

In reality, complexes are not always existing as pure single state. Some complexes exhibit, however, a spin-crossover phenomenon caused by external stimuli such as temperature, pressure and photo irradiation. The phenomenon is quite important in biological systems because it is closely-linked to the functional tuning processes in enzymatic cycles catalyzed by heme proteins. There are three types of spin-crossover processes; the spin-crossover between $S = 5/2$ and $S = 1/2$(type-1), $S = 3/2$ and $S = 1/2$(type-2), and $S = 5/2$ and $S = 3/2$(type-3) (Scheme 1).

Among the heme related complexes, the type-1 spin-crossover was discovered by Beetlestone and co-workers back in 1964 [1]. This type-1 spin crossover between the $S = 5/2$ and $S = 1/2$ has been most extensively studied in six-coordinated complexes such as $[Fe(OEP)(3\text{-}ClPy)_2]^+$ [2], $[Fe(TPP)(N_3)_2]$ [3], and $[Fe(OEP)(N_3)(1\text{-}MeIm)]$ [4, 5], while the type-2 spin-crossover was only recently found by ourselves in 2001 [6, 7]. As for the type-3 spin-crossover, no example has ever been reported until recently. Actually, the mixed $S = 5/2, 3/2$ spin state is considered to be a quantum mechanical spin admixture rather than the thermal equilibrium between two different spin states [8, 9].

In the course of the study, we and others clarified that the non-planarity of the heme is one of the key-factors to control the functions in the model heme complexes [10, 11]. And the importance of the non-planarity of the heme, which was found in naturally occurring hemeproteins, is further emphasized by the findings of the conservation of the distortion modes in the same functional proteins from different species as reported by Shelnutt and co-workers [12]. Thus, the deformation modes of heme are closely connected to the heme electronic structure regulated by the d_π-p_π interactions among iron(III) d-orbitals, frontier orbitals of the porphyrin ring and axial ligands [13, 14].

In accordance with the above mentioned fascinating features of the heme, we established a system to manipulate these spin-crossover phenomena of the iron(III) heme by using the combination of heme deformation, axial ligand field, electronic nature of the peripheral substituents, and so on. Thus, "The Spin-crossover Triangle in Iron(III) Heme" has been completed [1–9, 15]. In this review, the authors describe an overview of the spin-crossover triangle of the iron(III) heme and the response of the heme electronic structure to the external stimuli.

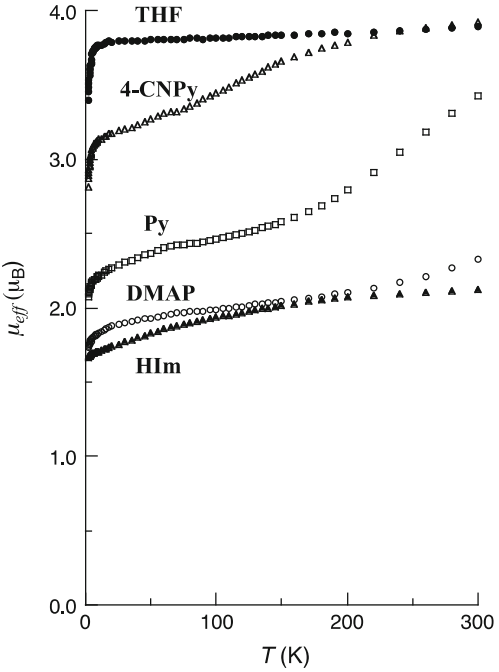

Figure 1 Temperature dependence of the effective magnetic moments of $[Fe(OETPP)L_2]^+$, where L are HIm(▲), DMAP(◯), Py(□), 4-CNPy(△), and THF(●), taken for microcrystalline samples by SQUID magnetometry

Table 1 Mössbauer parameters of a series of $[Fe(OETPP)L_2]^+$

Ligands		T/*K*	IS/*mm s*$^{-1}$	QS/*mm s*$^{-1}$	Spin state
THF		290	0.41	3.65	3/2
		80	0.50	3.50	3/2
4-CNPy	Site A	290	0.37	3.26	3/2
	Site A	80	0.57	3.03	3/2
	Site B	80	0.20	2.70	1/2
Py		290	0.32	2.76	3/2, 1/2
		80	0.25	2.29	1/2
DMAP		290	0.19	2.21	1/2
		80	0.26	2.31	1/2

Source: Ref. [6]

2 Spin-crossover between $S = 3/2$ and $S = 1/2$

2.1 SQUID magnetometry

Among the 6-coordinated porphyrin complexes, the combination of a highly saddled porphyrin, such as OETPP, with comparatively weak-field axial ligands produces spin-crossover complexes between $S = 3/2$ and $S = 1/2$ [6, 7].

Figure 1 shows the temperature dependence of the effective magnetic moments of a series of $[Fe(OETPP)L_2]^+$ complexes. The field strength of the axial ligands is in the order of HIm > DMAP > Py > 4-CNPy > THF. The results indicate that $[Fe(OETPP)(HIm)_2]^+$ and $[Fe(OETPP)(DMAP)_2]^+$ are in the low-spin state,

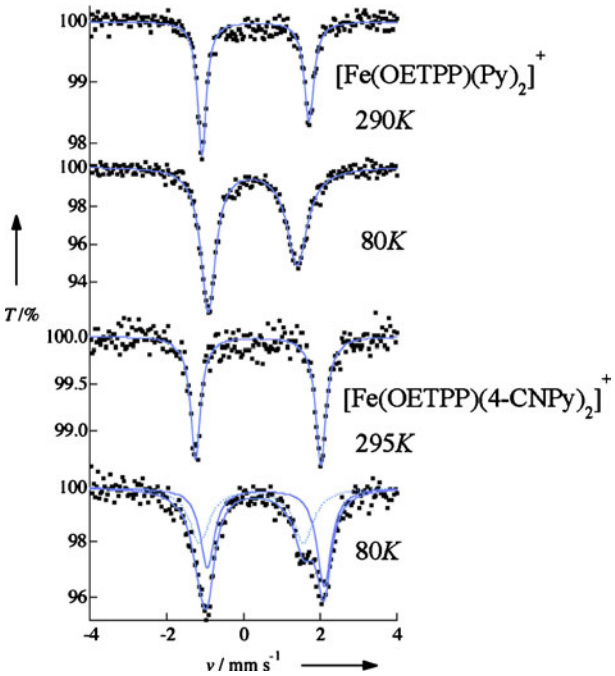

Figure 2 ^{57}Fe Mössbauer spectra of $[Fe(OETPP)(Py)_2]^+$ and $[Fe(OETPP)(4\text{-}CNPy)_2]^+$ at ambient temperature and 80 *K*. The Site A and Site B of $[Fe(OETPP)(4\text{-}CNPy)_2]^+$ at 80 K are expressed in *solid line* and *dotted line*, respectively

while the $[Fe(OETPP)(THF)_2]^+$ complex is in the quite pure intermediate-spin state over a wide range of temperatures. The complexes with comparatively weak-field ligands, $[Fe(OETPP)(4\text{-}CNPy)_2]^+$ and $[Fe(OETPP)(Py)_2]^+$, show the spin-crossover behavior between $S = 3/2$ and $S = 1/2$. While the $[Fe(OETPP)(Py)_2]^+$ complex exists as an exclusively low-spin species below 100 *K*, the fraction of the intermediate-spin species is gradually increasing when the temperature is raised from 100 *K* to 300 *K*. In a similar fashion, the $[Fe(OETPP)(4\text{-}CNPy)_2]^+$ complex exists as a thermal equilibrium mixture of the intermediate spin species and the low-spin species below 220 *K*. The complex, however, exists as an almost pure intermediate-spin species above 220 *K*.

2.2 Mössbauer spectra

Table 1 lists the Mössbauer parameters, IS(isomer shift) and QS(quadrupole splitting) measured at ambient temperature and 80 *K*, of a series of the $[Fe(OETPP)L_2]^+$ complexes. Also, ^{57}Fe Mössbauer spectra of $[Fe(OETPP)(Py)_2]^+$ and $[Fe(OETPP)(4\text{-}CNPy)_2]^+$ are shown in Fig. 2.

The IS and QS values for $[Fe(OETPP)(THF)_2]^+$ at both temperature indicate that the complex is in an almost pure intermediate spin state. Correspondingly, the IS and QS values for $[Fe(OETPP)(4\text{-}CNPy)_2]^+$, 0.37 and 3.26 $mm\ s^{-1}$, at ambient temperature suggest that the complex is in an intermediate spin state. In contrast, the IS and QS values for $[Fe(OETPP)(DMAP)_2]^+$ at ambient temperature indicate that the complex is in the $S = 1/2$ state. It is noteworthy that the Mössbauer parameters for $[Fe(OETPP)(Py)_2]^+$ at ambient temperature are between those of the

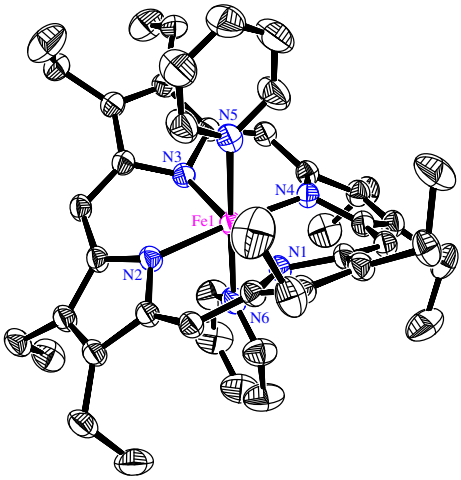

Figure 3 ORTEP diagrams of $[Fe(OETPP)(Py)_2]^+$. Thermal ellipsoids are drawn at the 30% probability level

$[Fe(OETPP)(THF)_2]^+$ and $[Fe(OETPP)(DMAP)_2]^+$, indicating that the complex exists as a thermal mixture of the intermediate spin species and the low spin species. The IS and QS values for $[Fe(OETPP)(DMAP)_2]^+$ at 80 *K*, 0.26 and 2.31 *mm* s^{-1}, indicate that the complex maintains its low spin state during the temperature change. On the other hand, when the temperature is lowered to 80 *K*, another newly produced doublet (Site B) is appearing in addition to the initial component (Site A) in the Mössbauer spectra of the $[Fe(OETPP)(4\text{-}CNPy)_2]^+$. The IS and QS values for Site A and Site B are, 0.57 and 3.03 *mm* s^{-1}, 0.20 and 2.70 *mm* s^{-1}, respectively. The result clearly indicates that the complexes are in a spin-crossover process between $S = 3/2$ and $S = 1/2$. On the contrary, for the $[Fe(OETPP)(Py)_2]^+$ complex, only one doublet is observed throughout the temperature range. The IS and QS values decrease to 0.25 and 2.27 *mm* s^{-1}, which indicates that the complex is in an almost low spin state at 80 *K*. So, the observed spin-crossover phenomena for both $[Fe(OETPP)(4\text{-}CNPy)_2]^+$ and $[Fe(OETPP)(Py)_2]^+$ are essentially similar, but there is a difference in the exchange speed in the thermal equilibrium process in the Mössbauer time scale, 10^{-7} s^{-1}.

2.3 Mechanistic aspect of the spin-crossover process

Crystallographic studies are extremely advantageous to clarify the mechanisms during the spin-crossover process. But, in general, it is quite difficult to observe the influence of a structural change in a spin-crossover process, since spin-crossover processes are often accompanied by a structural phase transition.

In the case of $[Fe(OETPP)(Py)_2]^+$, however, a temperature dependent X-ray structure analysis has been successfully carried out at 80, 180, and 298 *K* [7]. Due to a temperature change from 298 to 80 *K*, the volume of the unit cell shows a contraction of about 6.7%.

Figure 3 shows the molecular structure of $[Fe(OETPP)(Py)_2]^+$, which clearly exhibits a highly saddled structure. The maximum deviation from the mean $C_{20}N_4Fe$ plane is 1.312(3) Å for one of the β-pyrrole carbon atoms. The deviation of *meso* carbons from the mean porphyrin plane is 0.05 Å, which indicates that the complex

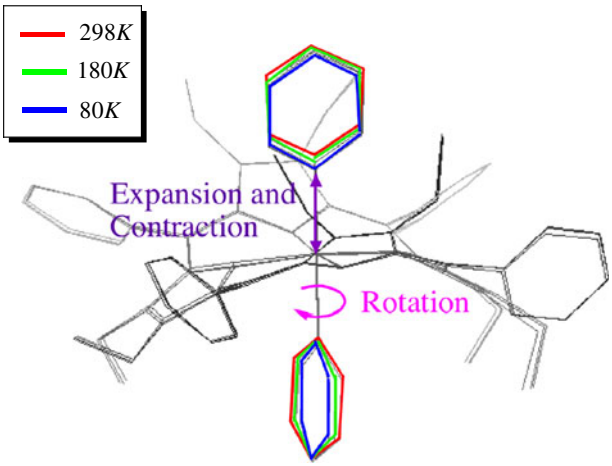

Figure 4 Temperature dependence of the structure in $[Fe(OETPP)(Py)_2]^+$

adopts a pure saddled deformation. A contraction of the axial bonds and the equatorial bonds is observed as the temperature is lowered. The average axial bond lengths, Fe-N_{ax}, at 298 *K*, 180 *K*, and 80 *K* are 2.201(3)Å, 2.041(4)Å, and 1.993(3)Å, respectively. Corresponding average equatorial bond lengths, Fe-N_p, are 1.985(3)Å, 1.954(3)Å, and 1.957(3)Å, respectively. The bond contraction between 298 and 180 *K* is much larger than that between 180 and 80 *K*; the bond contractions for the Fe-N_{ax} are 0.160 and 0.048 Å for each temperature range, respectively, while those for the Fe-N_p are 0.031 and <0.01 Å. Another notable change in structure is the rotation angle ϕ of the pyridine ligand; ϕ is defined as the dihedral angle between the coordinated pyridine plane and N_p-Fe-N_p. The pyridine ligands are placed almost along the diagonal N_p-Fe-N_p axes perpendicularly above and below the porphyrin; the average ϕ is fairly small, 2.4°, at 298 *K*. On cooling the crystal, the rotation angle increases from 2.4° to 6.0°, and then to 9.7°. The increase in the rotation angle can be ascribed to the contraction of the Fe-N_{ax} bond at lower temperature. Because of the bond contraction, the steric repulsion between the axial pyridine ligands and porphyrin ring should increase. Thus, the axial pyridine ligands rotate around the Fe-N_{ax} bond to minimize the steric repulsion. The mechanism of the spin-crossover process associated with the above-mentioned structural changes is explained as follows. As the temperature is lowered, the dynamics of the molecules, especially in the peripheral substituents, is restrained. Consequently, the molecules inside the crystal suffer chemical pressure from the neighboring molecules. As a result, the iron-nitrogen bonds are contracting especially in axial direction, since the complex is readily compressed in the axial direction due to the long Fe-N_{ax} bond. It should be noted that the crystallographic b-axis is almost coinciding with the Fe-N_{ax} bond, indicating a small tilt angle of about 15°. Hence, a larger contraction of the lattice constant is observed for the b-axis than for the a- and c- axes on cooling the crystal. These results clearly indicate that the contraction of the axial bonds is closely related to the mechanism of the spin-crossover between $S = 3/2$ and $S = 1/2$. Namely, the contraction of the axial bonds destabilizes the d_{z2} orbital and induces a spin transition from $S = 3/2$ to $S = 1/2$. The structural changes during the spin-crossover process between $S = 3/2$ and $S = 1/2$ are summarized in Fig. 4.

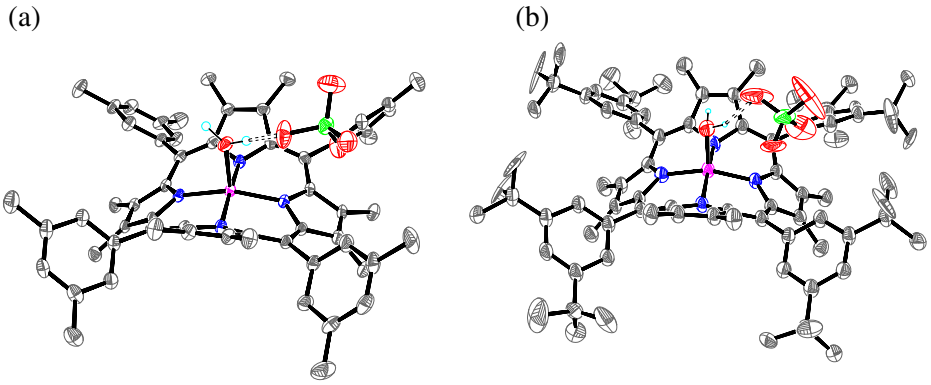

Figure 5 Molecular structures of $[Fe(OMTArP)(H_2O)]ClO_4$ **a** Ar = 3,5-Me_2Ph and **b** 3,5-^{t}Bu$_2$Ph. Ellipsoids are colored in *grey* (carbon), *blue* (nitrogen), *red* (oxygen), *green* (chlorine), *cyan* (hydrogen), and *magenta* (iron). Hydrogen bonds are shown as *dotted lines*

Table 2 Comparison of geometric parameters in 5-coordinated saddle shaped iron (III) porphyrin complexes

Complex	Fe-N_p[a)]	Fe-X_{ax}[b)]	ΔFe[c)]	N4 area[d)]	S[e)]	Ref
$[Fe(OMTArP)(H_2O)]^+$						
Ar=3,5-Me_2Ph	1.946(4)	2.084(4)	0.285(2)	7.45	3/2	[15]
Ar=3,5-^{t}Bu$_2$Ph	1.960(2)	2.056(2)	0.232(1)	7.59	3/2	[15]
Fe(OMTPP)Cl	2.034	2.247	0.464	7.87	5/2	[18]
Fe(OETPP)Cl	2.030	2.242	0.467	7.83	5/2	[18]
Fe(OETPP)ClO_4	1.963	2.059	0.262	7.59	3/2	[19]

a) Bond length (Å) between iron and pyrrole nitrogen. b) Bond length (Å) between iron and axial ligand. c) Out-of-plane deviation (Å) of iron (III) ion from the N_4 plane. d) The area (Å^2) of the plane consisting of the nitrogen atoms of the pyrrole rings. e) Spin state at ambient temperature

3 Spin-crossover between $S = 5/2$ and $S = 3/2$

A wide variety of research has been carried out on the spin transition in naturally occurring heme proteins because of its relevance to the important functional tuning process. While spin transitions between $S = 5/2$ and $S = 1/2$, and between $S = 3/2$ and $S = 1/2$ have been observed both in heme proteins and model heme complexes, the spin transition between $S = 5/2$ and $S = 3/2$ has never been observed before. In fact, the mixed $S = 5/2$ and $S = 3/2$ spin state is considered to be a quantum mechanical spin admixture caused by the spin-orbit coupling between $S = 3/2$ and $S = 5/2$ spin states [8, 9]. The structurally similar highly saddled mono aqua complexes, $[Fe(OMTArP)(H_2O)]ClO_4$, where Ar is 3,5-dimethylphenyl(3,5-Me_2Ph) and 3,5-bis(tert-butyl)phenyl(3,5-^{t}Bu$_2$Ph), however, exhibit the unprecedented example showing the spin transition between $S = 3/2$ and $S = 5/2$ spin states [15]. Shortly thereafter, several reports regarding spin-crossover between $S = 5/2$ and $S = 3/2$ have been published [16, 17].

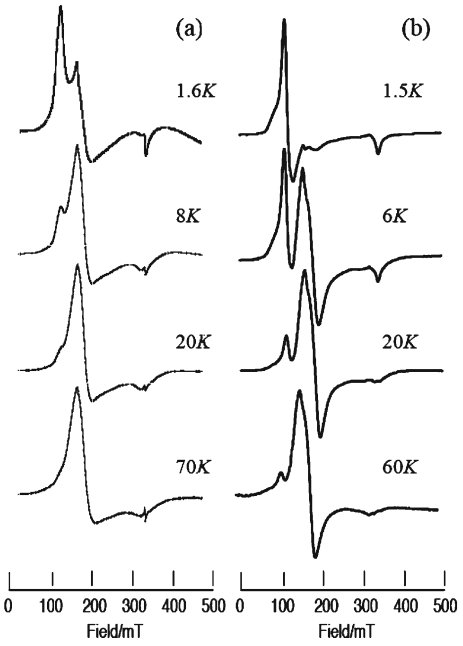

Figure 6 EPR spectra of $[Fe(OMTArP)(H_2O)]ClO_4$ **a** Ar = 3,5-Me_2Ph and **b** 3,5-$^{t}Bu_2$Ph taken in the solid at various temperatures

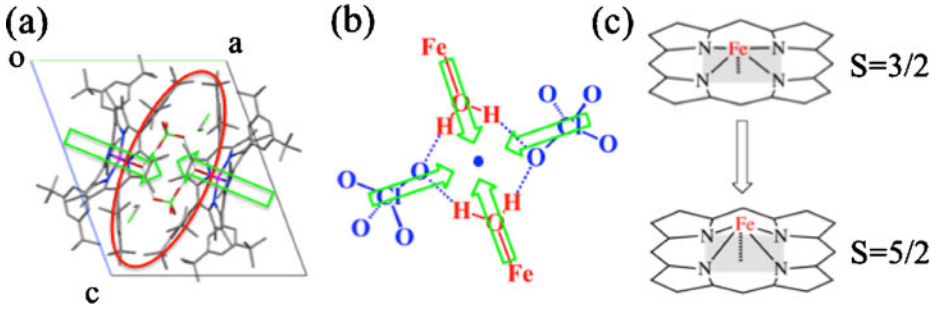

Figure 7 Structural change of $[Fe(OMTArP)(H_2O)]ClO_4$, where Ar = 3,5-$^{t}Bu_2$Ph, during the spin-crossover process between $S = 5/2$ and $S = 3/2$

3.1 X-ray structure analysis

Figure 5 shows the molecular structure of the 3,5-Me_2Ph and 3,5-$^{t}Bu_2$Ph complexes. The complexes adopt highly saddled deformations with deviations from the least-squares plane equal to 1.32–1.35 Å at the pyrrole-β carbons for both complexes. Table 2 shows the geometric parameters of these complexes together with some analogous complexes [15–17]. Significantly short Fe-N_p bond lengths and the extremely small distance of the iron from the N4 plane, ΔFe, observed in the $[Fe(OMTArP)(H_2O)]ClO_4$, which is comparable to those of $Fe(OETPP)ClO_4$, clearly indicate that these complexes are in the intermediate spin state.

3.2 EPR spectra

Temperature dependent EPR spectra of $[Fe(OMTArP)(H_2O)]ClO_4$, (a)Ar=3,5-Me_2Ph and (b) 3,5-^{t}Bu$_2$Ph, are given in Fig. 6.

Both complexes show similar temperature dependence of the spectra in the solid state. The EPR spectra at low temperature exhibit two types of signals, which are characteristic for high spin and intermediate spin species. The *g* values, determined by computer simulations of the observed spectra, are as follows: $[Fe(OMTArP)(H_2O)]ClO_4$ (a) Ar=3,5-Me_2Ph: 6.10, 5.90, 2.00 ($S = 5/2$), and 4.20, 3.80, 2.10 ($S = 3/2$); (b) 3,5-^{t}Bu$_2$Ph: 6.10, 5.90, 2.00 ($S = 5/2$), and 4.37, 3.77, 1.99 ($S = 3/2$). To our great surprise, the signal intensities for the intermediate-spin species increased, while those for the high-spin species decreased as the temperature was raised. Thus, both 3,5-Me_2Ph and 3,5-^{t}Bu$_2$Ph complexes exist exclusively as intermediate spin complexes above 70 *K*.

The phenomenon is observed reversibly during the temperature change. The temperature dependence of the EPR spectra clearly indicates that the complexes are in the spin-crossover process between $S = 5/2$ and $S = 3/2$. The van't Hoff plots yield ΔH° and ΔS° values corresponding to the equilibrium given in (1) to be 112 $J{\cdot}mol^{-1}$ and 52 $J{\cdot}mol^{-1}{\cdot}K^{-1}$ for the 3,5-Me_2Ph complex, and 100 $J{\cdot}mol^{-1}$ and *19* $J{\cdot}mol^{-1}{\cdot}K^{-1}$ for the 3,5-^{t}Bu$_2$Ph complex, respectively.

$$\text{High Spin} \underset{\rightleftharpoons}{\overset{K}{=}} \text{Intermediate Spin} \tag{1}$$

3.3 Mechanistic implication

As for crystal packing, the 3,5-Me_2Ph complex has a one-dimensional hydrogen bonding channel along a-axis. Contrary, the 3,5-^{t}Bu$_2$Ph complex exists as a discrete dimeric structure connected by hydrogen bonding shown in Fig. 7a and b.

The mechanisms of this spin-crossover process can be explained in terms of the difference in the molecular structure and crystal structure between ambient temperature and low temperature. At ambient temperature, the axial ligand water molecule, the counter perchlorate anion and the crystal solvent are highly disordered because of the thermal motion. But at extremely low temperature, those dynamics should settle down. The resultant vacant space (red circle in the Fig. 7a) should be filled by the rearrangement of the molecules as shown in green allows in the Fig. 7a. These movements, which correspond to the contraction of the hydrogen bond network around the symmetry center, induce the extruding rearrangement of the iron from the N4 plane in Fig. 7b and c. The resulting large out of plane displacement of the iron(III) ion can stabilize the d_{x2-y2} orbital and induce the spin transition from $S = 3/2$ to $S = 5/2$.

Acknowledgements This work was supported by Research Promotion Grants from the Toho University Graduate School of Medicine (Nos. 05-21 and 06-01 to Y.O.) and by Grant- in-Aid for Scientific Research from the Ministry of Education, Culture, Sports, Science and Technology, Japan (No. 18655025, 20550068 and 23550083 to Y.O.). This work was also supported by the Research Center for Materials with Integrated Properties, Toho University and Advanced Medical Research Center, Toho University. We also thank the Instrument Center of Institute for Molecular Science (IMS), Japan Synchrotron Radiation Research Institute (RIKEN, JASRI, SPring-8), and Photon Factory, High Energy Accelerator Research Organization (PF, KEK). The authors are grateful to

Mr. Motoyasu Fujiwara and Mr. Tadashi Ueda of the IMS for the assistance with the EPR and SQUID measurements.

References

1. Beetlestone, J., George, P.: Biochemistry **3**, 707 (1964)
2. Scheidt, W.R., Geiger, D.K., Haller, K.J.: J. Am. Chem. Soc. **104**, 495 (1982)
3. Ellison, M.K., Narsi, H., Xia, Y.-M., Marchon, J.-C., Schulz, C.E., Debrunner, P.G., Scheidt, W.R.: Inorg. Chem. **36**, 4804 (1997)
4. Neya, S., Tsubaki, M., Hori, H., Yonetani, T., Funasaki, N.: Inorg. Chem. **40**, 1220 (2001)
5. Neya, S., Chang, C.K., Okuno, D., Hoshino, Y., Hata, M., Funasaki, N.: Inorg. Chem. **44**, 1193 (2005)
6. Ikeue, T., Ohgo, Y., Yamaguchi, T., Takahashi, M., Takeda, M., Nakamura, M.: Angew. Chem. Int. Ed. **40**, 2617 (2001)
7. Ohgo, Y., Ikeue, T., Nakamura, M.: Inorg. Chem. **41**, 1698 (2002)
8. Maltempo, M.M., Moss, T.H., Cusanovich, M.A.: Biochim. Biophys. Acta **342**, 290 (1974)
9. Maltempo, M.M.: J. Chem. Phys. **61**, 2540 (1974)
10. Nakamura, M., Ohgo, Y., Ikezaki, A.: Electronic and magnetic structures of iron porphyrin complexes. In: Kadish, K.M., Smith, K.M., Guilard, R. (eds.) Handbook of Porphyrin Science, vol. 7, pp. 1–146. World Scientific, Singapore (2010)
11. Walker, F.A.: Proton NMR and EPR spectroscopy of paramagnetic metalloporphyrins. In: Kadish, K.M., Smith, K.M., Guilard, R. (eds.) The Porphyrin Handbook, vol. 5, pp. 81–183. Academic Press, San Diego, CA (2000)
12. Hobbs, J.D., Shelnutt, J.A.: J. Protein. Chem. **14**, 19–25 (1995)
13. Cheng, R.-J., Chen, P.-Y., Lovell, T., Liu, T., Noodleman, L., Case, D.A.: J. Am. Chem. Soc. **125**, 6774 (2003)
14. Conradie, J., Ghosh, A.: J. Phys. Chem. B. **107**, 6486 (2003)
15. Ohgo, Y., Chiba, Y., Hashizume, D., Uekusa, H., Ozeki, T., Nakamura, M.: Chem. Commun. (18), 1935–1937 (2006). doi:10.1039/b601412g
16. Neya, S., Takahashi, A., Ode, H., Hoshino, T., Hata, M., Ikezaki, A., Ohgo, Y., Takahashi, M., Hiramatsu, H., Kitagawa, T., Furutani, Y., Kandori, H., Funasaki, N., Nakamura, M.: Eur. J. Inorg, Chem., **20**, 3188 (2007)
17. Neya, S., Takahashi, A., Ode, H., Hoshino, T., Ikezaki, A., Ohgo, Y., Takahashi, M., Hiramatsu, H., Kitagawa, T., Furutani, Y., Lórentz-Fonfría, V.A., Kandori, H., Teraoka, J., Funasaki, N., Nakamura, M.: Bull. Chem. Soc. Jpn. **81**, 136 (2008)
18. Cheng, R.-J., Chen, P.-Y., Gau, P.-R., Chen, C.-C., Peng, S.-M.: J. Am. Chem. Soc. **119**, 2563 (1997)
19. Barkigia, K.M., Renner, M.W., Fajer, J.: J. Porphyr. Phthalocya. **5**, 415 (2001)